Tailoring Silver Nanodots for Intracellular Staining

Sungmoon Choi[a], **Junhua Yu**[a,‡], **Sandeep A. Patel**[a], **Yih-Ling Tzeng**[b,*], and **Robert M. Dickson**[a,*]

[a]School of Chemistry and Biochemistry and Parker H. Petit Institute for Bioengineering and Bioscience, Georgia Institute of Technology, 901 Atlantic Drive, Atlanta, GA 30332-0400 (USA)

[b]Department of Medicine, Emory University School of Medicine, Atlanta, GA 30322

Abstract

Through tailored oligonucleotide scaffolds, Ag nanocluster syntheses have yielded thermally and cell culture stable silver cluster-based emitters. Optimizing ssDNA stability has enabled creation of highly concentrated and spectrally pure nanocluster emitters with strong intracellular emission. Both fixed and live-cell staining become possible, and intracellular delivery is demonstrated both through conjugation to cell penetrating peptides and via microinjection.

Introduction

The outstanding one- and two photon absorption cross sections and photostabilities of DNA-encapsulated, few-atom silver nanoclusters suggest both additional single molecule and cellular applications of these novel fluorophores.[1–5] Though bare silver nanodots have been prepared within rare gas[6, 7] or zeolite matrices,[8–10] their utility as fluorescent labels at ambient conditions has only become possible upon encapsulation in water-soluble molecular scaffolds. Although successfully encapsulated in dendrimers,[11] microgels,[12] and peptides,[13] the single stranded DNA (ssDNA) scaffolds with varying sequences[1–4, 14–17] have, to date, produced the widest variety of and most robust nanodot emitters. Encapsulated within ss-DNA, few-atom Ag nanoclusters ("nanodots") exhibit excellent brightness with typical fluorescence quantum yields of ~30% and extinction coefficients exceeding $2 \times 10^5 M^{-1} cm^{-1}$.[2]

Combined with >10-fold photostability improvements over dyes such as Cy3, Cy5, and Texas Red;[2] small overall size; and two-photon cross sections[3] that can approach those of much larger quantum dots,[18, 19] these emitters fill a void between organics and much larger semiconductor-based fluorophores.[1, 13, 18–20]

Silver nanodots are generally synthesized by reduction of a mixture of ligand and silver nitrate by sodium borohydride.[1] The optimal nucleobase:silver ratio to yield maximized emission is usually found to be ~two bases per silver.[1, 2, 14, 16, 20–22] For a given sequence, however, variations in this ratio can bias fluorophore creation toward one of multiple emitters formed in a given sequence. Gwinn *et al*., for example, nicely illustrated this concept using DNA hairpins of varying length, but at constant Ag concentration, thereby yielding mixtures of multiple Ag nanodot emitters.[4, 16] Although recent successes at creating spectrally pure emitters have been achieved,[2, 23] most studies continue to result in low concentration mixtures of green and red emitters. Further, the extreme insolubility of Ag salts in biological media, coupled with poor spectral purity and low overall obtainable

*dickson@chemistry.gatech.edu . *ytzeng@emory.edu .
‡Current address: Department of Chemistry & Education, Seoul National University, Seoul 151–742, South Korea.

nanodot concentrations (i.e. sub-submicromolar)[4, 16, 21, 22, 24, 25] has precluded more widespread use of these otherwise promising fluorophores. Herein, through facile optimization of creation conditions, we create and utilize a wide range of multicolor fluorophores with excellent chemical stability and spectral purity, at sufficiently high concentrations for use in complex biological environments. These emitters can be delivered into living cells either by microinjection or through conjugation to a cell penetrating peptide (CPP),[26, 27] thereby opening paths toward intracellular labeling.

Results and discussion

Tuning the base:Ag^+ ratio away from the maximized 2:1[21] that simultaneously produces multiple emitters in the C_{20} oligocytosine sequence enables selective preparation of essentially spectrally pure emitters within C_{20} scaffolds. Upon increasing the base/Ag^+ ratio from 2 to more than 2.7, the previously reported, primarily red emission[1, 21, 22] transforms within 48 hours to yield a stable, spectrally pure green emitter (523 nm at λex 467 nm, Figure 1A) with a fluorescence lifetime of 3.6 ns and quantum yield of 27%. This emitter has a different excitation spectrum and photophysical parameters from those of other Ag nanodots previously reported.[21] Formation of this particular species is accelerated upon heating to 40 °C, yielding the pure green emitter within 6 hrs. This species has very good thermal stability, with a half life of more than two days when held at 60 °C. It also shows 55 excellent stability in chloride-containing buffers (Table 1). Interestingly, changing the oligocytosine length to 12 or 24 bases when formed with a ratio of 2.7 bases:Ag^+, or increasing the base/Ag^+ ratio up to 3.5 also produces a similar spectrally pure green emitter (>150-fold brighter than any other species in solution). Although several-fold lower than for other nanodots with near IR exctiation,[3] this Ag nanocluster exhibits a more than 100-fold larger two photon absorption cross section (4000 GM at 750 nm, (Goppert-Mayer units, 10^{-50} cm4 photon s^{-1})) over that of fluorescein (37 GM),[28] with excellent photostability, while retaining reasonably small size.[2]

Although a promising green emitter is obtained using C_{20}, sequence modifications are even more crucial than base:Ag ratio for tuning Ag nanodot emission color and spectral purity. Fine-tuning of creation conditions, coupled with optimizing the DNA hairpin sequence and thermal stability yield significant improvements in nanodot properties that enable intracellular use. Building on others' successful hairpin studies,[4] adding four complementary bases at the 3′ end of oligocytosine to yield $CGCGC_{12}$ (5′-CGCGCCCCCCCCCCCC <u>CC</u>GCG-3′) forms a stem-loop structure in which direct nanodot synthesis produces a spectrally pure 615 nm emitter at a loop base/Ag^+ ratio of 1.8, yielding a Φ_F nearly twice that of C_{12} nanodots (42% vs. 23%), and improved overall emission intensity relative to that obtainable in C_{12} (5′- CCCCCCCCCCCC-3') scaffolds (Figure 1B). Further, in contrast to C_{12}-encapsulated nanodots, the improved stability enables these emitters to be directly concentrated through either solvent evaporation or ethanol precipitation without destroying their stability or spectral purity. Such concentration was not possible with previous emitters that report the μM-encapsulating DNA concentration, but have very low nanodot yields.[22] These improved methods yield solutions with optical densities well above 3 (Figure 1C), indicating nanodot concentrations in excess of 10 μM. Analogous sequences with terminal hairpin structures, such as 20 $AATTC_{12}$, 5′-CGAACCCCCCCCCCCCTTCG-3′ ($CGAAC_{12}$), $ATATC_8$, and 5′-GGGGCCCCCCCCCCCCCC-3′ ($GGGGC_8$), also produce various spectrally pure, concentratable Ag nanodot solutions with very bright, spectrally pure emission with a ratio versus other observed emission of more than 100 and much higher concentrations than reported with any other hairpin or non-hairpin equivalent (Table 1). Interestingly, mismatched stem pairs (e.g. 5′-CGGCC$_{12}$CGCG-3′) fail to produce Ag nanodots at high concentrations (not shown), suggesting that the hairpin structure is beneficial to Ag nanodot formation[4] as also suggested with Ag-induced hairpin formation

within polycytosine.[29] Tuning the hairpin structure yields multiple spectrally pure emitters with emission wavelengths varying from the yellow to the red (Figure 1A). Each of these emitters exhibits excellent photophysics (Table 1) with photostabilities and sustained emission rates improving on the best available organic fluorophores.[30] As we report here, maintaining the oligocytosine loop, while increasing thermal stability of the stem and optimizing creation conditions has yielded buffer- and culture medium-stable emitters that maintain their strong emission for many hours at 37 °C (Figure 1D). With sub-3-nm hydrodynamic radii (data not shown) dominated by the encapsulating DNA strands, all emitters are likely composed of fewer than ~10 Ag atoms,[31] although chemical analysis of these hairpins remains elusive. However, no nanoparticle formation is observed in any of these samples either with darkfield imaging or centrifugation at 23,000 g. Although concentration enables highly absorbing, spectrally pure (>100 fold higher than any other emitter) solutions to be obtained, chemical synthetic yields for these emitters only range from 1% to 5%, depending on the sequences. Clearly higher yield synthetic methods will further improve imaging applications.

Even without hairpin-based stabilization, the spectrally pure, green-emitting C_{20}:Ag nanodots selectively stain the nuclei of fixed NIH3T3 cells (Figure 2) and show excellent photostability under both one- and two-photon excitation. These cells were co-stained with HCS red cell stain (Invitrogen), which stains the cytoplasm, as shown in red. Under confocal scanning, both labels show excellent one-photon-excited stability, with less than 10% fluorescence intensity decay of either dye after 2 hrs of continuous imaging (Figure 2A,C). However, under two-photon-excitation (TPE), the fluorescence intensity of HCS red decays to 60% after just 10 min of scanning, while Ag nanodots retain 90% fluorescence intensity after scanning for 1 hr (Figure 2B,D). The *in vitro* one- and two-photon excited nanodot emission spectra, excited at 458 nm (OPE) or at 720 nm (TPE), respectively, are indistinguishable (not shown).

Upon conjugation to an antibody, Ag nanodots do not significantly impair specificity. $AATTC_{12}$ was conjugated to anti-HS to mark the cell membrane, and red emitting $ATATC_8$ was conjugated to anti-OP to mark the mitochondria. Methods analogous to those previously reported were followed. Upon conjugation and nanocluster formation in $AATTC_{12}$, emission is blue-shifted by 40 nm to 522 nm, but the conjugated $ATATC_8$ Ag nanodot emission is unchanged. As shown in Figures 2E&F, methanol-fixed NIH 3T3 cells treated with anti-OP/$ATATC_8$ Ag nanodots (5 μM, concentration of DNA ligand) and anti-HS/$AATTC_{12}$ Ag nanodots (5 μM, concentration based on DNA ligand) stained mitochondria (red) and the cell membrane (green), respectively. The strong staining of nuclei observed with unconjugated green nanodots was circumvented with antibody conjugation.

Ag salts are notoriously insoluble, but all of these Ag nanodot emitters are highly buffer stable. Prepared directly in PBS, the green C_{20} nanodots show excellent chemical stability in both PBS and in DMEM cell growth medium under ambient conditions. This C_{20}-encapsulated green emitter is actually preferentially stabilized in PBS. The combination of thermal and buffer stability suggest that the DNA performs a significant protecting role in this nanodot emitter, as other C_{20}-encapsulated emitters are destabilized under these buffer conditions, leading to spectral shifts and eventual cluster decay.[22] The balance between improved DNA stabilization at high ionic strength,[32–34] and the insolubility of most Ag salts preferentially forms this green emitter in a variety of buffers composed from sodium bicarbonate, sodium acetate, or sodium perchlorate. The stability decreases somewhat with increased temperature, retaining half of its emission in DMEM after 4 hours at 60 °C. We should note that shorter oligocytosine-protected Ag nanodots (e.g. C_{12}) possess similar thermal and chemical stability only in the absence of high concentration of chloride.

Live cell imaging with Ag nanodots also poses significant challenges. The excellent chemical stability offered by hairpin-encapsulated Ag nanodots, however, enables direct preparation in DMEM and significantly improved stability in cell culture without apparent silver salt precipitates during nanodot formation. For these syntheses, $AgNO_3$ is directly added to DMEM solutions containing the hairpin of interest, followed by chemical reduction. Using $ATATC_{12}$, direct nanocluster preparation in DMEM produces emitters with greatly improved stability compared to those prepared with the same sequence in regular phosphate buffer at 4 °C. It is likely that those with stable DNA-Ag^+ complexes are chemically pre-selected during the incubation of DNA-Ag^+ prior to chemical reduction, yielding stable emission. However, those unstable DNA-Ag^+ complexes could not form silver nanodots. To further improve the nanodot thermal stability in high salt conditions, we increased the stem length in the hairpin structure for nanodot preparation directly in DMEM. Employing 5′-CGAACGCGC$_{12}$CGCGTTCG-3′ (hairpin melting temperature (T_m) of 72 °C),[35] bright 618 nm emission with excellent stability in PBS as well as DMEM at 37 °C is observed with a half life of 5 hrs. This is more than two-fold improved over the $ATATC_{12}$ encapsulated silver nanodots (Figure 1E).

Since the high charge density of DNA limits intracellular availability, and endosomal escape when using transfection reagents is often a problem,[36, 37] both microinjection and cell penetrating peptide (CPP) conjugation were utilized for cytosolic delivery. Although highly cargo dependent in subcellular localization, CPPs have been demonstrated to effectively import small cargoes ranging from fluorophores to oligos and small proteins.[38, 39] Large cargo such as quantum dots, however, are unable to reach the cytosol upon CPP conjugation.[40] As a proof-of-concept, we conjugated a commonly employed CPP, penetratin,[41] to oligocytosine ssDNA scaffolds for nanodot delivery. Penetratin is derived from the third helix of the Antennapedia homeodomain and has been widely investigated for cargo delivery due to its low cytotoxicity and high delivery efficiency.[38, 39, 42, 43] Three glycines and one cysteine were added to the C-terminus of the penetratin peptide to yield RQIKIWFQNRRMKWKKGGGC, in which the thiol group can be tethered to amino-group-functionalized oligocytosines (Integrated DNA Technologies, Coralville, IA, USA) through the heterobifunctional cross-linker sulfo-SMCC to yield conjugate penetratin-C_{12}. The oppositely-charged penetratin and ssDNA tend to form aggregates due to electrostatic interaction, mandating use of high NaCl concentration (1 M) and high temperature (60 °C) during synthesis. The resulting conjugate and emissive nanodots also require high ionic strength for solubility (1 M sodium acetate). Only short (and therefore less anionic) strands yielded good conjugation efficiencies, dictating conjugation with C_{12} for nanodot formation. Red-emitting Ag nanodots were formed within this penetratin-C_{12} conjugate by mixing with silver nitrate in aqueous sodium acetate solution, followed by borohydride reduction at a base:silver ratio of 2:1. The resulting penetratin-C_{12} Ag nanodots possess the essential photophysical properties of ssDNA-encapsulated Ag nanodots, i.e, 640 nm emission at 575 nm excitation (Figure 1E),[21] indicating that the electrostatic interaction between penetratin and ssDNA does not interfere with the formation and photophysics of the Ag nanodots.

Cargo delivery was examined using NIH 3T3 cells and bovine pulmonary artery endothelial cells (BPAEC). Penetratin-C_{12} Ag nanodots (10 μM) initially bind with and eventually cross the cell membrane, with silver nanodots being readily detected in nuclei within 10 min either in NIH 3T3 or BPAEC cells (Figure 3A and D, respectively), with some expected residual membrane staining.[44] The DNA-encapsulated Ag nanodots alone showed no staining of cells (data not shown), indicating penetratin-dependent cellular uptake. The internalization of penetratin-C_{12} Ag nanodots ceases at 4 °C, which is in line with reports that endocytosis may be involved in CPP translocation.[39] Further, the penetratin-C_{12} Ag nanodots entered cells with intact cell membranes, as demonstrated by co-incubation of penetratin-C_{12} Ag nanodots with the cell membrane-impermeable dye Sytox Green (Invitrogen) which only

stains nuclei of cells with compromised membranes (Figure 3B,C). In all the Ag nanodotstained cells, less than 15% of cells showed poor cell membrane integrity. Though the challenge of charge compensation limits solubility and size of penetratin-DNA conjugates, this demonstrates that intracellular imaging studies with ssDNA encapsulated Ag nanodot fluorophores indeed hold promise.

Conversely, direct microinjection circumvents difficulties in membrane transport and the problem of endosomal escape. Microinjection (Eppendorf FemtoJet) of concentrated 615 nm ($CGCGC_{12}$) emitting nanodots into live NIH 3T3 cells, for example, demonstrates the ability of these Ag nanodots to show bright red fluorescence in the cytosol, and indicates promise for more generalized cellular staining using these or similar nanodot probes (Figure 3E and F), as stability is also further improved. Although eventually higher fluorescence intensity is observed in the nucleus even with microinjected Ag nanodots after 10 minutes, the distribution of fluorescence is initially almost exclusively cytosolic. This distribution appears uninfluenced by the Ag cluster, as fluorescein-tagged ssDNA of the same sequence exhibits a similar distribution inside living cells.

Experimental

I) *Chemicals*. Silver nitrate (99.9999%), phosphate buffered saline (PBS), ethylenediaminetetraacetic acid (EDTA), Trypsin, Dulbecco's Modified Eagle's Medium (DMEM), sodium borohydride, sulfo-SMCC (4-(NMaleimidomethyl)cyclohexane-1-carboxylic acid 3-sulfo-N-hydroxysuccinimide ester sodium salt), tris(2-15 carboxyethyl)phosphine, penicillin-streptomycin solution, and Sephadex G50 were purchased from Sigma-Aldrich and used as received. 3,000 MWCO centrifugal ultrafiltration vials were obtained from Vivascience, Stonehouse, UK. ssDNAs were synthesized by Integrated DNA Technologies. Antiheparin/heparan sulfate mouse IgG1 (anti-HS) was obtained from Millipore, MA, USA, and anti-OxPhos complex IV subunit Va mouse IgG2a (anti-OP) from Invitrogen, CA, USA.

II) *Cell culture*. NIH 3T3 cells were incubated under 5% carbon dioxide/air at 37 °C, in DMEM with 4.5 g/L glucose, L-glutamine and pyruvate, supplemented with 10% newborn bovine serum and 1% penicillin/100 units streptomycin mixture. Bovine pulmonary artery endothelial cells (BPAEC) were cultured in M199 medium with Earle's salts, supplemented with 20% fetal bovine serum and 1% penicillin/streptomycin, fungizone (2.5 μg/ml) and endothelial cell growth supplement (17 μg/mL).

III) *Fluorescence and MALDI spectra*. Fluorescence spectra were taken on a Photon Technology International spectrofluorometer (QM-4SE). MALDI mass spectra were run on the Applied Biosystems 4700 Proteomics Analyzer.

IV) *Two-photon cross sections*. The absorption cross section was determined by recording the emission as a function of excitation wavelength by a pulsed Ti-sapphire laser (200 fs pulse width, 8kHz repetition rate). The cross sections were measured by ratiometric comparison to dye standards with known cross sections at the excitation wavelengths used, analogous to our previously reported methods.[3]

V) *Cellular staining*. NIH 3T3 cells were washed with PBS and then fixed with pre-cooled MeOH/acetone (−20 °C) for 10 min, rinsed with deionized water, and then loaded with anti-mitochondria (anti-OP) $ATATC_8$ (5'-ATATCCCCCCCC ATAT-3') silver nanodots (5 μM) in 300 μL of DI water for 1 hr at r.t. The cells

were then washed and incubated with anti-HS AATTC$_{12}$ (5'-ATATCCCCCCCCCCCCATAT-3') silver nanodots (5 μM) in 300 μL of DI water for 1.2 hrs. Cells were washed with deionized water and then mounted on a slide for imaging.

VI) *Live cells* were loaded with penetratin-C$_{12}$ silver nanodots in modified phosphate buffer (110 mM sodium phosphate, 2.7 mM potassium phosphate, and 5 mM MgCl$_2$, pH 7.45) for 10 min in an incubator, washed with modified phosphate buffer, and mounted on a slide for imaging.

VII) *Molar extinction coefficients* were determined by fluorescence correlation spectroscopy with appropriate color laser excitation on nanodot solutions of known dilution from those with measurable nanodot-specific absorbance. The number of molecules in the laser focal volume was obtained from the y-intercept of the correlation function,[45, 46] and the focal volume determined by measuring known concentrations of standard organic dyes. Together, accounting for dilution, these values directly yield the nanodot molar extinction coefficient.[47]

VIII) *Synthesis of penetratin-C$_{12}$.* C$_{12}$ functionalized with an amino group (5′-AmMC12-CCCCCCCCCCCC-3′, 6 mg, IDT DNA) was stirred with sulfo-SMCC (8 mg, Aldrich) in sodium borate buffer (0.1 M, pH 8.5) at r.t. for 3 hrs. The resulting maleimide-modified C$_{12}$ was purified over a Sephadex G-50 column with degassed PBS as the eluant. The collected DNA was then mixed in 1 M NaCl with penetratin that has reacted with 5 mM Tris(2-carboxyethyl)phosphine (2 mL) for 3 hrs and purified over a Sephadex G-50 column. After 4 hrs at 60 °C, the product was purified over a SP Sephadex column (SPC50-120, Aldrich) with borate buffer 10 mM phostate, 150 mM NaCl, 200 mM sodium borate, pH 7.8) as the eluant, with a final product yield of 35% based on DNA absorption. MS (MALDI): m/z 6324 calculated for C$_{239}$H$_{355}$N$_{76}$O$_{100}$P$_{12}$S$_2$ found 6327 ([M+Na]$^+$).

IX) *Synthesis of silver nanodots.* For green emitting silver nanodot preparation, ssDNA and silver nitrate were mixed at a base /Ag$^+$ ratio of 2.7, followed by aqueous sodium borohydride solution (1 mg/mL) reduction at a NaBH$_4$/Ag$^+$ molar ratio of 1 under vigorous stirring. The emission shifts to green within 48 hours. For hairpin DNA-protected silver nanodots, ssDNA and silver nitrate were mixed at a loop base /Ag$^+$ ratio of 1.8, and reduced by sodium borohydride reduction at a NaBH$_4$/Ag$^+$ ratio of 1. All other non-hairpin DNA-protected silver nanodots were synthesized by mixing silver nitrate and ssDNA at a base / Ag$^+$ ratio of 2, followed by aqueous sodium borohydride solution reduction at a NaBH$_4$/Ag$^+$ ratio of 1.

Conclusions

These improvements in chemical, biological, and thermal 100 stabilities, coupled with spectral purity and high concentrations obtained in ssDNA hairpin-encapsulated nanoclusters have retained the outstanding Ag nanodot optical properties, but now offer promise for more demanding intracellular applications. Cellular delivery demonstrates strong nanodot fluorescence in the live cells, with further opportunities for improvement and utilization for studying protein dynamics with fluorescence labeling.

Acknowledgments

Notes and references

1. Petty JT, Zheng J, Hud NV, Dickson RM. DNA-templated Ag nanocluster formation. J. Am. Chem. Soc. 2004; 126:5207–5212. [PubMed: 15099104]

2. Richards CI, Choi S, Hsiang JC, Antoku Y, Vosch T, Bongiorno A, Tzeng YL, Dickson RM. Oligonucleotide-stabilized Ag nanocluster fluorophores. J. Am. Chem. Soc. 2008; 130:5038–5039. [PubMed: 18345630]

3. Patel SA, Richards CI, Hsiang JC, Dickson RM. Water-soluble Ag nanoclusters exhibit strong two-photon-induced fluorescence. J. Am. Chem. Soc. 2008; 130:11602–11603. [PubMed: 18686957]

4. O'Neill PR, Velazquez LR, Dunn DG, Gwinn EG, Fygenson DK. Hairpins with Poly-C Loops Stabilize Four Types of Fluorescent Ag-n:DNA. J. Phys. Chem. C. 2009; 113:4229–4233.

5. Xu HX, Suslick KS. Water-Soluble Fluorescent Silver Nanoclusters. Adv. Mater. 2010; 22:1078–1082. [PubMed: 20401932]

6. Felix C, Sieber C, Harbich W, Buttet J, Rabin I, Schulze W, Ertl G. Ag-8 fluorescence in argon. Phys. Rev. Lett. 2001; 86:2992–2995. [PubMed: 11290090]

7. Haslett TL, Bosnick KA, Moskovits M. Ag-5 is a planar trapezoidal molecule. J. Chem. Phys. 1998; 108:3453–3457.

8. Sun T, Seff K. Silver clusters and chemistry in zeolites. Chem. Rev. 1994; 94:857–870.

9. De Cremer G, Antoku Y, Roeffaers MBJ, Sliwa M, Van Noyen J, Smout S, Hofkens J, De Vos DE, Sels BF, Vosch T. Photoactivation of silver-exchanged zeolite A. Angew. Chem.-Int. Edit. 2008; 47:2813–2816.

10. Harbich W, Fedrigo S, Meyer F, Lindsay DM, Lignieres J, Rivoal JC, Kreisle D. Deposition of mass selected silver clusters in rare gas matrices. J. Chem. Phys. 1990; 93:8535–8543.

11. Zheng J, Dickson RM. Individual water-soluble dendrimer-encapsulated silver nanodot fluorescence. J. Am. Chem. Soc. 2002; 124:13982–13983. [PubMed: 12440882]

12. Zhang JG, Xu SQ, Kumacheva E. Photogeneration of fluorescent silver nanoclusters in polymer microgels. Adv. Mater. 2005; 17:2336–2340.

13. Yu J, Patel SA, Dickson RM. In vitro and intracellular production of peptide-encapsulated fluorescent silver nanoclusters. Angew. Chem.-Int. Edit. 2007; 46:2028–2030.

14. Guo WW, Yuan JP, Dong QZ, Wang EK. Highly Sequence-Dependent Formation of Fluorescent Silver Nanoclusters in Hybridized DNA Duplexes for Single Nucleotide Mutation Identification. J. Am. Chem. Soc. 2010; 132:932–934. [PubMed: 20038102]

15. Shang L, Dong SJ. Facile preparation of water-soluble fluorescent silver nanoclusters using a polyelectrolyte template. Chem. Commun. 2008:1088–1090.

16. Gwinn EG, O'Neill P, Guerrero AJ, Bouwmeester D, Fygenson DK. Sequence-dependent fluorescence of DNA-hosted silver nanoclusters. Adv. Mater. 2008; 20:279–283.

17. Koszinowski K, Ballweg K. A Highly Charged Ag-6(4+) Core in a DNA-Encapsulated Silver Nanocluster. Chem.-Eur. J. 2010; 16:3285–3290.

18. Larson DR, Zipfel WR, Williams RM, Clark SW, Bruchez MP, Wise FW, Webb WW. Water-soluble quantum dots for multiphoton fluorescence imaging in vivo. Science. 2003; 300:1434–1436. [PubMed: 12775841]

19. Clapp AR, Pons T, Medintz IL, Delehanty JB, Melinger JS, Tiefenbrunn T, Dawson PE, Fisher BR, O'Rourke B, Mattoussi H. Two-photon excitation of quantum-dot-based fluorescence resonance energy transfer and its applications. Adv. Mater. 2007; 19:1921–1926.

20. Yu JH, Choi S, Dickson RM. Shuttle-Based Fluorogenic Silver-Cluster Biolabels. Angew. Chem.-Int. Edit. 2009; 48:318–320.

21. Ritchie CM, Johnsen KR, Kiser JR, Antoku Y, Dickson RM, Petty JT. Ag nanocluster formation using a cytosine oligonucleotide template. J. Phys. Chem. C. 2007; 111:175–181.

22. Antoku, Y. Ph. D thesis. Georgia Institute of Technology; 2007. Fuorescent Polycytosine-Encapsulated Silver Nanoclusters.

23. Patel SA, Cozzuol M, Hales JM, Richards CI, Sartin M, Hsiang JC, Vosch T, Perry JW, Dickson RM. Electron Transfer-Induced Blinking in Ag Nanodot Fluorescence. J. Phys. Chem. C. 2009; 113:20264–20270.

24. Sharma J, Yeh HC, Yoo H, Werner JH, Martinez JS. A complementary palette of fluorescent silver nanoclusters. Chem. Commun. 2010; 46:3280–3282.

25. Yu JH, Choi SM, Richards CI, Antoku Y, Dickson RM. Live Cell Surface Labeling with Fluorescent Ag Nanocluster Conjugates. Photochem. Photobiol. 2008; 84:1435–1439. [PubMed: 18764887]

26. Terrone D, Sang SLW, Roudaia L, Silvius JR. Penetratin and related cell-penetrating cationic peptides can translocate across lipid bilayers in the presence of a transbilayer potential. Biochemistry. 2003; 42:13787–13799. [PubMed: 14636045]

27. Turner JJ, Ivanova GD, Verbeure B, Williams D, Arzumanov AA, Abes S, Lebleu B, Gait MJ. Cell-penetrating peptide conjugates of peptide nucleic acids (PNA) as inhibitors of HIV-1 Tat-dependent trans-activation in cells. Nucleic Acids Res. 2005; 33:6837–6849. [PubMed: 16321967]

28. Albota MA, Xu C, Webb WW. Two-photon fluorescence excitation cross sections of biomolecular probes from 690 to 960 nm. Appl. Optics. 1998; 37:7352–7356.

29. Freeman R, Finder T, Willner I. Multiplexed Analysis of Hg^{2+} and Ag^+ Ions by Nucleic Acid Functionalized CdSe/ZnS Quantum Dots and Their Use for Logic Gate Operations. Angew. Chem.-Int. Edit. 2009; 48:7818–7821.

30. Schmidt T, Kubitscheck U, Rohler D, Nienhaus U. Photostability data for fluorescent dyes: An update. Single Mol. 2002; 3:327.

31. Petty JT, Fan C, Story SP, Sengupta B, John Iyer A, Prudowsky Z, Dickson RM. DNA Encapsulation of 10 Silver Atoms Producing a Bright, Modulatable, Near-Infrared-Emitting Cluster. J.Physi. Chem. Lett. 2010:2524–2529.

32. Sorokin VA, Gladchenko GO, Valeev VA, Sysa IV, Petrova LG, Blagoi YP. Effect of salt and organic solvents on DNA thermal stability and structure. J. Mol. Struct. 1997; 408:237–240.

33. Szopa J. Effect of temporarily increased ionic-strength and of urea on stability of DNA complexes with native and acetylated BPTI. Arch. Immun. Ther. Exper. 1979; 27:131–140.

34. Schildkr C, Lifson S. Dependence of melting temperature of DNA on salt concentration. Biopolymers. 1965; 3:195–208. [PubMed: 5889540]

35. [Accessed on 10 August 2010] Trasition temperature was calculated based on Integrated DNA Technologies web source. Available at: http://www.idtdna.com/analyzer/Applications/OligoAnalyzer/.

36. Majumdar S, Duvvuri S, Mitra AK. Membrane transporter/receptor-targeted prodrug design: strategies for human and veterinary drug development. Adv. Drug Deliv. Rev. 2004; 56:1437–1452. [PubMed: 15191791]

37. Antoku Y, Hotta J, Mizuno H, Dickson RM, Hofkens J, Vosch T. Transfection of living HeLa cells with fluorescent poly-cytosine encapsulated Ag nanoclusters. Photochem. Photobiol. Sci. 2010; 9:716–721. [PubMed: 20442932]

38. Gratton JP, Yu J, Griffith JW, Babbitt RW, Scotland RS, Hickey R, Giordano FJ, Sessa WC. Cell-permeable peptides improve cellular uptake and therapeutic gene delivery of replication-deficient viruses in cells and in vivo. Nat. Med. 2003; 9:357–362. [PubMed: 12598894]

39. Thoren PEG, Persson D, Isakson P, Goksor M, Onfelt A, Norden B. Uptake of analogs of penetratin, Tat(48–60) and oligoarginine in live cells. Biochem. Biophys. Res. Commun. 2003; 307:100–107. [PubMed: 12849987]

40. Jablonski AE, Kawakami T, Ting AY, Payne CK. Pyrenebutyrate Leads to Cellular Binding, Not Intracellular Delivery, of Polyarginine Quantum Dots. J. Phys. Chem. Lett. 2010; 1:1312–1315. [PubMed: 20436938]

41. Derossi D, Joliot AH, Chassaing G, Prochiantz A. The 3rd Helix of the Antennapedia Homeodomain Translocates through Biological-Membranes. J. Biol. Chem. 1994; 269:10444–10450. [PubMed: 8144628]

42. Fischer R, Fotin-Mleczek M, Hufnagel H, Brock R. Break on through to the other side - Biophysics and cell biology shed light on cell-penetrating peptides. ChemBioChem. 2005; 6:2126–2142. [PubMed: 16254940]

43. Tripathi S, Chaubey B, Ganguly S, Harris D, Casale RA, Pandey VN. Anti-HIV-1 activity of anti-TAR polyamide nucleic acid coniugated with various membrane transducing peptides. Nucleic Acids Res. 2005; 33:4345–4356. [PubMed: 16077030]

44. Ziegler A, Nervi P, Durrenberger M, Seelig J. The cationic cell-penetrating peptide Cpp(TAT) derived from the HIV-1 protein TAT is rapidly transported into living fibroblasts: Optical, biophysical, and metabolic evidence. Biochemistry. 2005; 44:138–148. [PubMed: 15628854]

45. Elson EL, Magde D. Fluorescence correlation spectroscopy .1. conceptual basis and theory. Biopolymers. 1974; 13:1–27.

46. Magde D, Elson EL, Webb WW. Fluorescence correlation spectroscopy. 2. Experimental realization. Biopolymers. 1974; 13:29–61. [PubMed: 4818131]

47. Haustein E, Schwille P. Fluorescence correlation spectroscopy: Novel variations of an established technique. Annu. Rev. Biophys. Biomolec. Struct. 2007; 36:151–169.
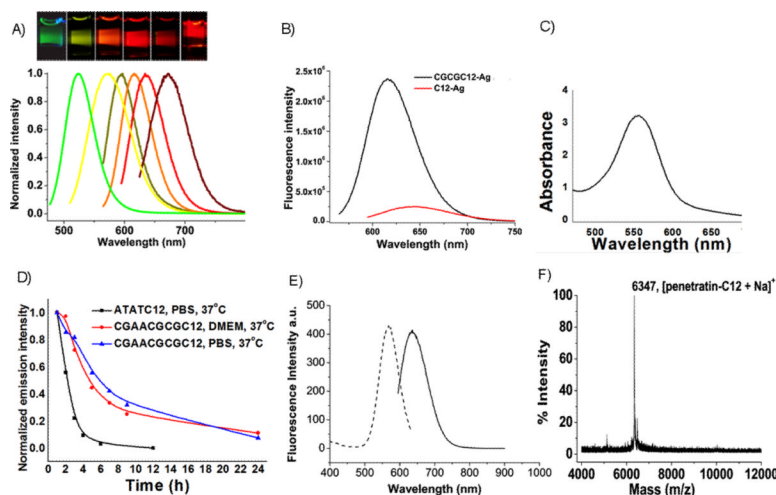
Fig. 1.
Emission and multicolor staining of various Ag nanodots. A, Normalized emission spectra of various emitters, from left to right: 523 nm (green C_{20}), 562 nm ($AATTC_{12}$), 590 nm ($CGAAC_{12}$), 615 nm ($CGCGC_{12}$), 635 nm ($ATATC_8$), 670 nm ($GGGGC_8$). (Inset) different color Ag emitters in cuvettes, each excited near their excitation maximum. B, Emission intensity comparison of Ag nanodots between sequence with a hairpin structure ($CGCGC_{12}$: 5'-CGCGCCCCCCCCCCCCCGCG-3') and that with a simple polycytosine structure (C_{12}: 5'-CCCCCCCCCCCC-3'), each at their highest intensities. C, Typical absorption spectrum of concentrated 615-nm emitter (1-cm light path). D, Thermal stability of $CGAACGCGC_{12}CGAACGCG$-protected Ag nanodots compared to $ATATC_{12}$-protected Ag nanodots. E, Excitation and emission spectra of aqueous penetratin-C_{12} silver clusters solution. Emission (solid) was excited at 575 nm, and excitation (dotted) was detected at 640 nm. F, MALDI mass spectrum of penetratin-C_{12} conjugate.
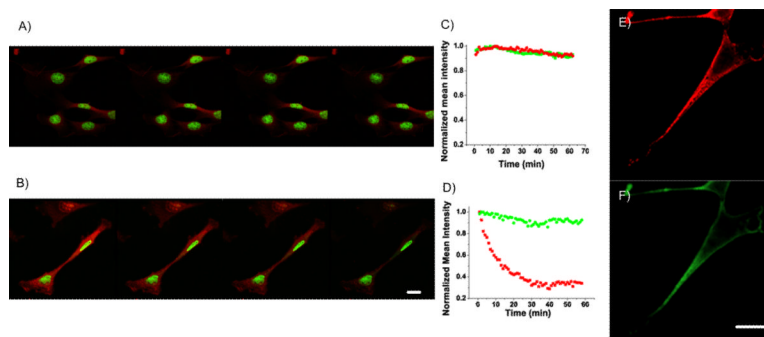
Fig. 2.
Confocal fluorescence imaging and photo-stability of C_{20} Ag nanodots (green) in NIH 3T3 cells co-labeled with HCS red cell stain (red) under one photon excitation (OPE, 458 nm, **A**) or two photon excitation (TPE, 720 nm, **B**). The photostability can be easily seen by the color decay of images in nuclei (green C_{20} Ag nanodots) and cytoplasm (HCS red cell stain), and illustrated in **C** (for OPE) and **D** (for TPE) by their mean fluorescence intensity of individual emitters in the corresponding scanning images. The green Ag nanodots show similar photostability to HCS red cell stain under OPE, but much greater stability under TPE. **E** and **F**, red and green channels from fixed NIH 3T3 cells co-stained with anti-OxoPhos/ATATC$_8$ Ag nanodots (red) and anti-Heparin Sulfate/AATTC$_{12}$ Ag nanodots (green). Scale bar, 30 μm.
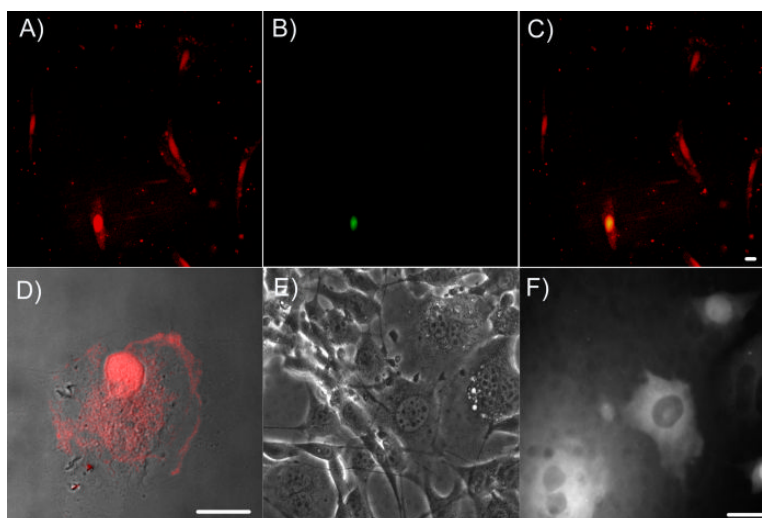
Fig. 3.
Intracellular delivery of DNA-encapsulated Ag nanodots. **A–D**, Penetratin-enhanced Ag nanodot internalization. **A** to **C**, colocalization of NIH 3T3 cells co-incubated with penetratin-C_{12} Ag nanodots and Sytox Green nuclear staining dye which only stains nuclei of cells with compromised membranes. The merge (**C**) of red emission (**A**) from penetratin-C_{12} Ag nanodots and green emission (**B**) from Sytox Green indicates that only a few cells show poor membrane integrity. Panels A–C are at the same scale. Penetratin-C_{12} Ag nanodots were excited at 543 nm and Sytox Green at 488 nm. **D**, Merge of a bright field image and a fluorescent image of BPAECs incubated with penetratin-C_{12} Ag nanodots for 10 min. **E** and **F**, 615 nm emitter was micro-injected into NIH 3T3 cells, shown in phase contrast (**E**) and fluorescence after microinjection (**F**). All scale bars are 25 µm.

Table 1

PhotoPhysical Parameters of Ag Nanodots

DNA sequence	T_m (°C)	Exc/Em (nm)	Lifetime (ns)	Φ (%)	E 10^5 $M^{-1}cm^{-1}$)	Half life time in water at 20 °C (hours)	Half life time in PBS at 37 °C (hours)
C_{20}	n/a	467/523	3.6 ± 0.1	27 ± 2	1.2 ± 0.3	>80	20
$AATTC_{12}$	9	480/562	4.3 ± 0.1	38 ± 3	2.0 ± 0.4	6	<1
$CGAAC_{12}$	32	543/590	2.0 ± 0.1	36 ± 3	3.5 ± 0.7	7	<1
$CGCGC_{12}$	57	560/615	2.5 ± 0.1	42 ± 3	9.5 ± 1.9	19	<1
$CGAACGCGC_{12}$	72	560/618	2.3 ± 0.1	16 ± 2	2.8 ± 0.6	40	6
$ATATC_8$	3	570/635	2.7 ± 0.1	26 ± 3	3.2 ± 0.7	5	<1
$GGGGC_8$	64	600/670	3.5 ± 0.1	34 ± 3	2.5 ± 0.5	>40	<1